
AFFORDANCE-BASED ROBOT MANIPULATION WITH FLOW MATCHING

Fan Zhang, Michael Gienger
Honda Research Institute EU
firstname.lastname@honda-ri.de

September 4, 2024

ABSTRACT

We present a framework for assistive robot manipulation, which focuses on two fundamental challenges: first, efficiently adapting large-scale models to downstream scene affordance understanding tasks, especially in daily living scenarios where gathering multi-task data involving humans requires strenuous effort; second, effectively learning robot trajectories by grounding the visual affordance model. We tackle the first challenge by employing a parameter-efficient prompt tuning method that prepends learnable text prompts to the frozen vision model to predict manipulation affordances in multi-task scenarios. Then we propose to learn robot trajectories guided by affordances in a supervised Flow Matching method. Flow matching represents a robot visuomotor policy as a conditional process of flowing random waypoints to desired robot trajectories. Finally, we introduce a real-world dataset with 10 tasks across Activities of Daily Living to test our framework. Our extensive evaluation highlights that the proposed prompt tuning method for learning manipulation affordance with language prompter achieves competitive performance and even outperforms other finetuning protocols across data scales, while satisfying parameter efficiency. Learning multi-task robot trajectories with a single flow matching policy also leads to consistently better performance than alternative behavior cloning methods, especially given multimodal robot action distributions. Our framework seamlessly unifies affordance model learning and trajectory generation with flow matching for robot manipulation. <https://hri-eu.github.io/flow-matching-policy/>.

1 Introduction

Recent advances in vision-language models (VLMs) present unprecedented opportunities to solve robot manipulation problems. Attempts in the field have focused on three primary aspects: 1) End-to-end learning manipulation from scratch. These approaches [Padalkar et al., 2023] make the least assumptions on tasks and are formulated in language-image-to-action prediction models. 2) Off-the-shelf-vision-language models for robot manipulation. Such line of works have explored using pre-trained VLMs with prompt engineering in various contexts of robot motion learning, including reward design for reinforcement learning [Ma et al., 2023], python coding [Liang et al., 2023], joint actions [Wang et al., 2023], etc. 3) Intermediate substrate to bridge high-level language-image instructions and low-level robot policies. These works usually introduce some form of prior derived from human knowledge as an intermediate stage, including affordances [Huang et al., 2023], pre-trained visual representations [Xiao et al., 2022], primitive skills [Ingelhart et al., 2024], etc. In this paper, we follow the third line of work. We propose to learn manipulation affordances, leveraging finetuning vision-language foundation models with a wealth of internalized knowledge. Then the affordance model is used for learning low-level robot policies, and thus helps to alleviate the sample inefficiency problem of end-to-end learning from scratch.

Extracting affordance knowledge has long inspired the robot community [Xiao et al., 2022]. We particularly focus on affordance learning in multi-task scenarios with text prompting. As shown in Fig. 2, given the same visual scene but with different language instructions, we aim to extract different affordances for robot policy learning through our proposed model. To leverage the ability of pre-trained foundation models while avoiding expensive computational constraints, recent works have explored parameter-efficiently fine-tuning (PEFT) large vision-language models for

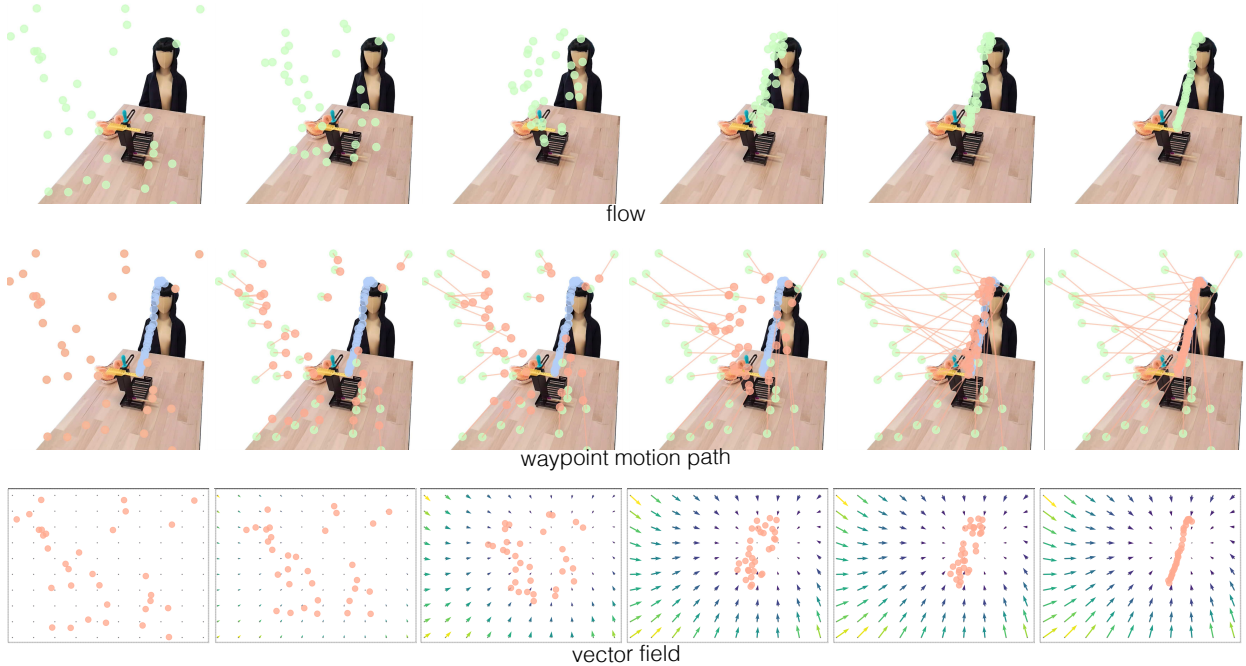


Figure 1: Flow Matching policy representations. The flow, waypoint motion path, and vector field are presented to showcase the process of flow matching transforming random waypoints to the target trajectory from timestep 0 to 1.

various visual recognition applications [Jia et al., 2022]. PEFT could be mainly categorized into two main groups: adapter-based methods (e. g., LoRA [Hu et al., 2021]) and prompt-based methods [Liu et al., 2023]. One representative line of such research has concentrated on prompt tuning methods, which prepend learnable prompts to the input of a large frozen pre-trained model and optimize them via gradients during finetuning. Studies on randomly-generalized trainable prompts [Jia et al., 2022] for universal use or condition-admitted prompt variables [Sohn et al., 2023] for better specific task performance have been both explored. It has shown that prompt tuning could match the performance of full finetuning but with substantially less parameter storage in various domains, including visual tracking [Zhu et al., 2023] and cross-domain tasks such as language-dance assessment [Zhong and Demiris, 2024]. Inspired in part by the notion of human cognitive penetrability mechanism [Maier and Abdel Rahman, 2019] that uses linguistic knowledge to tune ongoing visual processing, we incorporate learnable text-conditioned prompts in a frozen vision foundation model to learn instruction-relevant manipulation affordance.

The subsequent challenge involves deploying the visual affordance across various robot manipulation learning paradigms. From the traditional behavior cloning with convolutional networks [Zhang and Demiris, 2022] to transformer-based learning structures [Shridhar et al., 2023], extensive research has modeled robot action trajectories from visual scenes. A recent line of works builds on successes in diffusion models [Chi et al., 2023] to generate motion trajectories, to capture multimodal action distributions and stable training behavior. Flow Matching is another novel generative method. Sharing theoretical similarities with stochastic Denoising Diffusion Probabilistic Models, flow matching aims to regress onto a deterministic vector field to flow samples toward the target distribution. It has proven that the simplicity of flow matching objectives allows favorable performance in stable training and generation quality compared to solving complex stochastic differential equations in diffusion models. We extend flow matching to the robotics domain. This is the first attempt to leverage flow matching in real-world robot manipulation from visual affordance. As shown in Fig. 1 and Fig. 2, the proposed method would flow the random waypoints to the desired trajectories based on various affordances in a single flow matching policy.

We also construct a real-world dataset with 10 tasks across Activities of Daily Living to test the proposed method. The novelty of our dataset is that it contains same scenarios but with multi-task affordance and robot trajectories. Experimental evaluation empirically demonstrates that the prompt tuning method for learning affordances achieves performance competitive, and sometimes beyond other finetuning protocols across data scales, vision-language fusion architectures, and prompt variants. Furthermore, we showcase that flow matching policy attains favorable performance in stable training and generation quality amongst competing methods of robot behavior cloning. Note that our goal

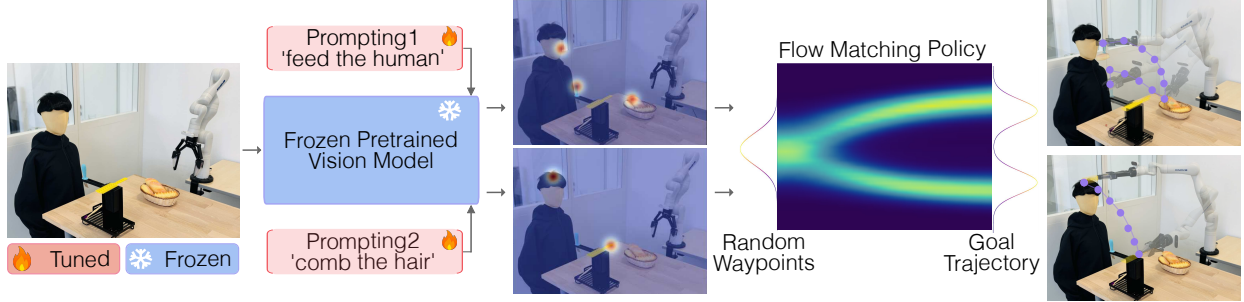


Figure 2: The proposed framework of unifying affordance model learning and trajectory generation for robot manipulation. Given the same visual scene but different language instructions, the model first extracts instruction-relevant manipulation affordances. This is achieved through a prompt tuning method that prepends learnable text-conditioned prompts in a frozen vision foundation model. Then a flow matching policy is proposed to transform the random waypoints to the desired trajectories, guided by task-relevant affordances.

is not to achieve the state-of-the-art general robot manipulation performance, but instead to broadly explore a new paradigm of efficiently adapting VLMs for affordance learning, and robot policy for multimodal action distributions.

The main contributions can be summarized as follows:

1. A parameter-efficient prompt tuning method for adapting pretrained vision foundation model conditioned on language instructions to learn manipulation affordances.
2. A novel formulation using Flow Matching for robot manipulation policy learning from visual affordances.
3. Empirical results investigating the advantages of the proposed algorithm on our constructed real-world robot multi-task dataset.

2 Related Work

2.0.1 Robot Learning from Demonstration

Imitation learning has been a common paradigm for robots which requires simulated or real-world demonstration data collection [Zhang and Demiris, 2023]. To improve data efficiency, extensive works have been proposed to learn robot policies on the top of visual representations [Liu et al., 2024] instead of end-to-end raw images [Goyal et al., 2023]. Keypoints or affordance heatmaps are often used to provide contact information as visual representation [Liu et al., 2024]. The concept of affordance has been introduced in [Gibson, 2014], referring to the ability to perform certain actions with objects in the context of a given scene. This paper concentrates on using affordances to guide the low level robot manipulation. In terms of network architectures for robot learning, prior works have successfully investigated convolutional networks [Zhang and Demiris, 2022], Transformers [Shridhar et al., 2023], generative adversarial networks [Ho and Ermon, 2016], Energy-Based Models [Florence et al., 2022], etc. However, the collected data is usually expected to be non-convex and multi-modal due to the variability in human demonstrations. Recent works have addressed this problem by reformulating the robot policy as a generative process. Diffusion policy [Chi et al., 2023] has emerged as a powerful class of generative models for behavior cloning by representing a robot’s visuomotor policy as a conditional denoising diffusion process. In this work, we investigate Flow Matching [Lipman et al., 2022], a novel generative model that has demonstrated its superiority in image generation, but is much less explored in robotics domains.

2.0.2 Parameter-Efficient Finetuning

Instruction-aware vision encoding [Gupta et al., 2022] has been extensively studied for various language-vision fusing tasks [Radford et al., 2021]. Given the dominance of large-scale vision-language models, many approaches have been proposed to efficiently finetune a frozen pretrained model for different downstream tasks to speed up training and reduce memory. Two representative methods among them are adapters and prompting. The first type of research varies depending on the adapter that could add extra lightweight modules [Gao et al., 2024] or express the weight updates as a low-rank decomposition of the weight matrix [Hu et al., 2021]. Another line of work focuses on prompting [Liu et al., 2023], which originally primes a frozen pretrained language model for downstream tasks by including a text prompt. Recent works on prompt tuning [Liu et al., 2021] treat prompts as continuous vectors and compute their gradients

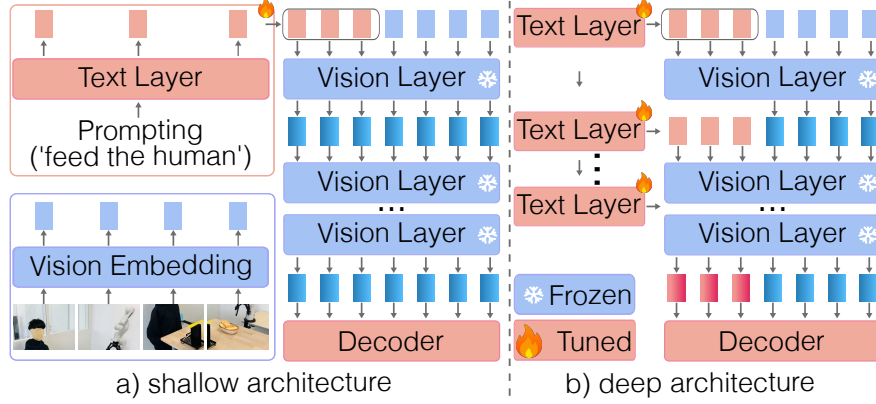


Figure 3: Overview of prompt tuning structures used for affordance learning. (Left) For the shallow structure, text-conditioned prompts are prepended to the first vision transformer layer. (Right) For the deep structure, prompts are inserted to every vision layer. Only the prompt-related layers and the decoder are being updated during the training, while the vision transformer remains frozen.

with backpropagation during training. The extension of prompt tuning to vision tasks has gained massive success. Visual prompt tuning [Jia et al., 2022] has manipulated visual prompts to steer models in arbitrary vision tasks. Other works [Sohn et al., 2023] have further explored extending the random learnable prompts to condition-based prompts (e. g., class, instance) that are hence less universal but more accurate. Inspired by its recent success, we extend the prompt tuning technologies to address the challenge of adapting large pretrained vision-language models to affordance learning for robot manipulation. The intuition is clear: if the model understands the posed text instruction and the inherent context, it should extract visual affordances that directly correspond to the relevant image aspects. Our method achieves the above goal by integrating learnable text-conditioned prompts into a large vision encoder, while keeping it frozen to preserve visual understanding capabilities.

2.0.3 Flow Matching in Robotics

Despite its recent progress in image generation [Albergo and Vanden-Eijnden, 2022], the application of flow matching in robotics domains remains underexplored. Few prior studies [Braun et al., 2024, Hu et al., 2024, Rouxel et al., 2024] have successfully modeled transformations that smoothly move random samples towards target robot actions. These works are nevertheless limited to simulation tasks or conditioned on state-based input. We propose the flow matching policy to learn multi-task robot behavior from raw images with visual affordances in a single supervised policy.

3 Methods

3.1 Prompt Tuning for Affordance Learning

Given a pre-trained vision transformer, our objective is to learn a set of text-conditioned prompts to maximize the likelihood of correct affordance labels, as shown in Fig. 3. Only the prompt-related layers and the decoder are being updated during the training, while the vision transformer remains frozen. Inspired by Vision Prompt Tuning [Jia et al., 2022], we also propose shallow and deep network architectures.

3.1.1 Shallow Architecture

The vision transformer layer takes the image patch embeddings \mathbf{E}_0 as input, and passes through various layers \mathbf{L}_i^v to achieve vision features \mathbf{E}_i , where $\mathbf{E}_i \in \mathbb{R}^{M \times C}$ and C is the channel dimension.

$$\mathbf{E}_i = \mathbf{L}_i^v(\mathbf{E}_{i-1}) \quad i = 1, 2, \dots, N$$

Similarly, the text transformer layer could be represented as

$$\mathbf{P}_i = \mathbf{L}_i^p(\mathbf{P}_{i-1}) \quad i = 1, 2, \dots, N$$

where \mathbf{P}_0 denotes the text tokens, text features \mathbf{P}_i are obtained through various layers \mathbf{L}_i^p , where $\mathbf{p}_i \in \mathbb{R}^{K \times C}$.

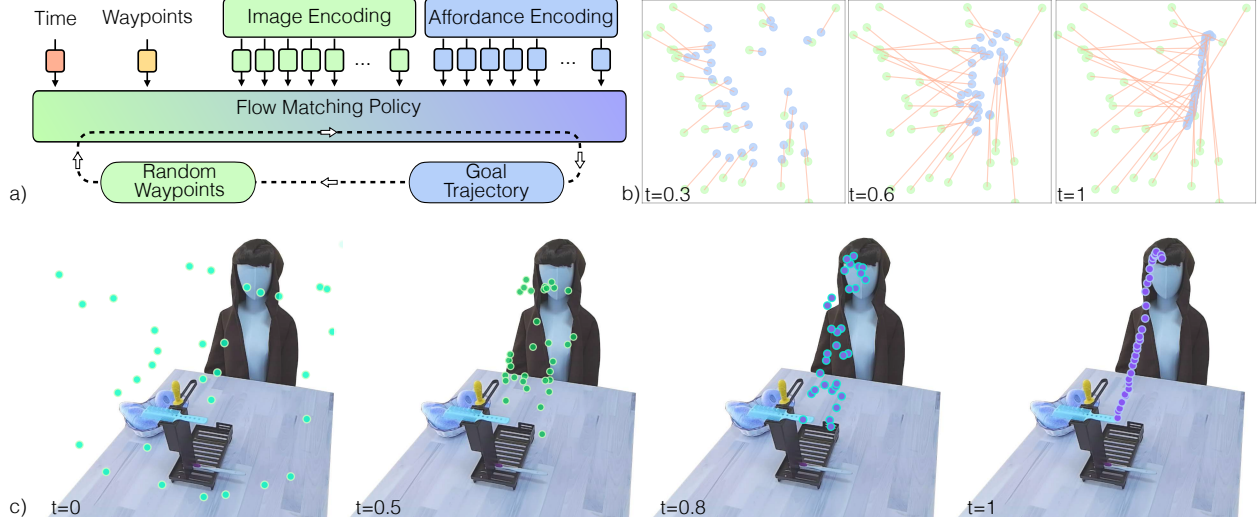


Figure 4: Framework of Flow Matching Policy. (a) At each time step, the policy predicts flow vectors for each waypoint conditioned on visual affordance observation data as well as the waypoints at the current timestep. (b-c) Flow matching transforms random waypoints (green) to the target trajectory (purple) from timestep 0 to 1. The lines in (b) denote the flow vectors.

As shown in Fig. 3, for the shallow structure, only one text transformer layer is used to compute text features P_1 , which are then treated as prompts and inserted into the first vision transformer Layer:

$$\begin{aligned} [Z_1, E_1] &= L_1^v([P_1, E_0]) \\ [Z_i, E_i] &= L_i^v([Z_{i-1}, E_{i-1}]) \end{aligned}$$

Then a decoder is added on the global output flattened token sequence to generate visual affordance tokens.

$$\text{Affordance} = \text{Decoder}(Z_N, E_N)$$

3.1.2 Deep Architecture

For the deep architecture, the only difference is that text features P_i are computed through each layer and introduced at the corresponding vision transformer layer’s input space:

$$\begin{aligned} [_, E_1] &= L_1^v([P_1, E_0]) \\ [_, E_i] &= L_i^v([P_i, E_{i-1}]) \end{aligned}$$

3.1.3 Implementation Details

We adopt the L2 Mean Squared loss between the predicted and ground truth affordances for network training. We add positional embeddings to all the image and language tokens to preserve the positional information. In the subsequent experiments, we will further study multiple model variants, including text and vision fusion, prompt depth, pretrained weights for vision transformer, etc.

3.2 Flow Matching Policy

In this session, we build the robot behavioral cloning policy as a generative process of Flow Matching, which constructs a flow vector that continuously transforms a source probability distribution towards a destination distribution. Flow Matching leverages an ordinary differential equation to deterministically mold data distribution, contrasting with diffusion policy which is based on a stochastic differential equation through introducing noise.

3.2.1 Flow Matching Model

Given a probability density path $p_t(\mathbf{x})$ and a corresponding vector field $\mathbf{u}_t(\mathbf{x})$, the objective loss of flow matching could be described as:

$$\mathcal{L}_{\text{FM}}(\boldsymbol{\theta}) = \mathbb{E}_{t, p_t(\mathbf{x})} \|\mathbf{v}_t(\mathbf{x}, \boldsymbol{\theta}) - \mathbf{u}_t(\mathbf{x})\|^2 \quad (1)$$

Algorithm 1 Flow Matching Policy**Input:** affordance observation \mathcal{O}_t , demonstrated robot trajectory \mathbf{x}_1 , source random waypoints p_0 **Output:** flow $\mathbf{v}_t(\mathbf{x}|\mathcal{O}_t)$ **while** not converged **do** $\mathbf{x}_0 \sim p_0$, sample random robot waypoints $t \sim \mathcal{U}[0, 1]$, sample time steps $\mathbf{x}_t = t\mathbf{x}_1 + (1-t)\mathbf{x}_0$, interpolate trajectories $\mathbf{v}_t(\mathbf{x}|\mathcal{O}_t) = f_\theta(\mathbf{x}_t, t|\mathcal{O}_t)$, flow estimation $\nabla_\theta \mathcal{L}_{\text{FM}}$, gradient step**end while**

where $\mathbf{x} \sim p_t(\mathbf{x})$, $t \sim \mathcal{U}[0, 1]$ (uniform distribution). The aim of flow matching is to regress $\mathbf{u}_t(\mathbf{x})$ with a time-dependent vector field of flow $\mathbf{v}_t(\mathbf{x}, \theta)$ parameterized as a neural network with weights θ . $\mathbf{u}_t(\mathbf{x})$ can be represented as

$$\mathbf{u}_t(\mathbf{x}) = \mathbf{x}_1 - \mathbf{x}_0 \quad \mathbf{x}_0 \sim p_0, \mathbf{x}_1 \sim p_1$$

p_0 represents a simple base density at time $t = 0$, p_1 denotes the target complicated distribution at time $t = 1$, \mathbf{x}_0 and \mathbf{x}_1 are the corresponding samplings. $\mathbf{v}_t(\mathbf{x}, \theta)$ could be described as:

$$\mathbf{v}_t(\mathbf{x}, \theta) = f_\theta(\mathbf{x}_t, t) \quad (2)$$

We define \mathbf{x}_t as the linear interpolation between \mathbf{x}_0 and \mathbf{x}_1 with respect to time $\mathbf{x}_t = t\mathbf{x}_1 + (1-t)\mathbf{x}_0$, following the Optimal Transport theory [Peyré et al., 2019]. And f_θ is a network of the flow model. Thus Equation (1) could be reformatted as:

$$\mathcal{L}_{\text{FM}}(\theta) = \mathbb{E}_{t, \mathbf{x}_0 \sim p_0, \mathbf{x}_1 \sim p_1} \|f_\theta(\mathbf{x}_t, t) - (\mathbf{x}_1 - \mathbf{x}_0)\|^2 \quad (3)$$

This represents the progression of the scalar flow that transforms data from source to target between time 0 and 1.

3.2.2 Flow Matching for Visuomotor Policy Learning

We extend flow matching to learn robot visuomotor policies. This requires two modifications in the formulation: i) changing the output \mathbf{x} to represent robot actions; ii) modeling the flow estimation conditioned on input image observations. Fig. 4 illustrates our model structures.

In our case of robot manipulation, \mathbf{x}_1 in Equation (3) represents the demonstration robot trajectories. \mathbf{x}_0 is the random generated waypoints following a multivariate normal distribution $\mathbf{x}_0 \sim \mathcal{N}(0, I)$. \mathbf{x} here denotes the complete long-horizon robot trajectory for various tasks. We modify Equation (2) as:

$$\mathbf{v}_t(\mathbf{x}|\mathcal{O}_t) = f_\theta(\mathbf{x}_t, t|\mathcal{O}_t)$$

3.2.3 Implementation Details

The whole training process of the flow matching policy is illustrated in Algorithm 1 and Fig. 4. At time step t , the policy predicts flow vectors \mathbf{v}_t for each waypoint conditioned on visual affordance observation data \mathcal{O}_t with Feature-wise Linear Modulation (FiLM) [Perez et al., 2018] as well as the waypoints at the current timestep \mathbf{x}_t . The visual embeddings \mathcal{O}_t are obtained through ResNet [He et al., 2016], and the flow model f_θ is represented with U-Net. We will ablate various structures later.

For the inference procedure, random waypoints are sampled from the source distribution and then flowed into the target trajectory by estimating the flow from $t = 0$ to $t = 1$ over single or several steps:

$$\mathbf{x}_{t+\Delta t} = \mathbf{x}_t + \Delta t f(\mathbf{x}_t, t|\mathcal{O}_t), \quad \text{for } t \in [0, 1] \quad (4)$$

4 Experiments

We systematically evaluate prompt tuning method and flow matching policy against baseline studies. We also investigate how design choices would affect their performance.

We construct a real-world dataset with 10 tasks across Activities of Daily Living to test the proposed method. Each task includes 1,000 sets of RGB images, demonstrated robot trajectories, and labeled ground truth of affordances. The data has been manually collected by moving robot end-effectors with kinesthetic teaching. The novelty of our dataset could be summarized as: (i) It contains same scenarios with multiple objects, multi-task affordances and the demonstrated

Methods		Learnable Params (M) ↓	Affordance Heatmaps ($\times 10^{-3}$) ↓	Heatmap Centers (pixel) ↓
Baselines	Full	153.8	0.76	1.15
	Decoder	3.9	1.51	13.48
	Adapter	19.2	1.17	6.22
	Cross-attention	43.5	1.26	8.89
	side-network	42.7	1.35	9.20
Ours	PT-shallow	8.0	1.42	12.04
	PT-deep (self-supervised weights)	42.1	0.80	2.93
Ablations	PT-deep (supervised weights)	42.1	1.48	10.13
	PT-deep (image output)	42.1	1.56	13.27

Table 1: Results of prompt tuning baseline and ablation studies. We report the number of learnable parameters, the heatmap estimation error (the fourth column) and the heatmap center error (the fifth column). Our method outshines other baselines except for the full finetuning.

robot trajectories. (ii) All tasks are related to Activities of Daily Living that involve (simulated) human data. The dataset will be made publicly available soon. More details about tasks and prompts can be found in supplementary materials. We randomly split the dataset with 80%-20% percentage of training and testing. The results reported here are obtained after 1,000 epochs of training with 3-fold cross validation. The inputs and outputs are normalized for network training, which are then mapped back to the original scale for results reporting.

Our tasks include prompt primitives: ‘sweep the trash’, ‘pass the water to the human’, ‘hang the towel’, ‘put on the hat’, ‘cover the food’, ‘wipe the nose’, ‘wipe the forearm’, ‘feed the human’, ‘comb the hair’, and ‘brush the teeth’. Each task corresponds to one prompt primitive. We could also add a pretrained LLM layer (e. g., GPT) in the front for zero-shot text classification, allowing for linking other language instructions to one of the ten prompt primitives.

4.1 Affordance Evaluation with Prompt Tuning

4.1.1 Experiment Setup and dataset

We use a pretrained ViT-B-16 transformer as a vision backbone. The text layer adopts the classic setup, including Multiheaded Self-Attention, Feed-Forward Networks with LayerNorm and residual connections. As suggested by MAE [He et al., 2022], the decoder is only used for downstream tasks, and could be flexible and lightweight. Thus we use one single transformer decoder layer. For a fair comparison, all the baselines here use self-supervised pretrained MAE weights on ImageNet-21k dataset for the vision transformer model. In ablation studies, we will investigate different pretrained weights. The training parameters for the prompt tuning network include an image size of 224×224 , AdamW with a learning rate of $1.5e-4$ including Warmup with step-decay, and batch size of 256. The text encoding layers output 76 tokens, as the CLIP method [Radford et al., 2021].

4.1.2 Baseline Studies

In this experiment, we benchmark our proposed shallow and deep prompt tuning structures against several commonly used finetuning and instruction-aware vision encoding protocols.

- Full finetuning: fully update the text and vision transformer layers and the decoder.
- Adapter-based methods: insert MLP layers with residual connections between pretrained frozen transformer layers of vision and language, as customary in the literature [Gao et al., 2024].
- Decoder-based methods: These methods treat the pretrained backbone as a feature extractor with fixed weights during tuning, and only the decoder is tuned, as customary in the literature [He et al., 2016].
- side-network methods: train a text transformer network on the side and append pretrained vision features and sidetuned text features before being fed into the decoder, as customary in the literature [Ganz et al., 2024].
- Cross-attention methods: Similarly to the above side-network methods, the difference here is using cross-attention fusing instead of simple prepending. An example of cross-attention fusing vision and language could be found in the literature [Jiang et al., 2022].

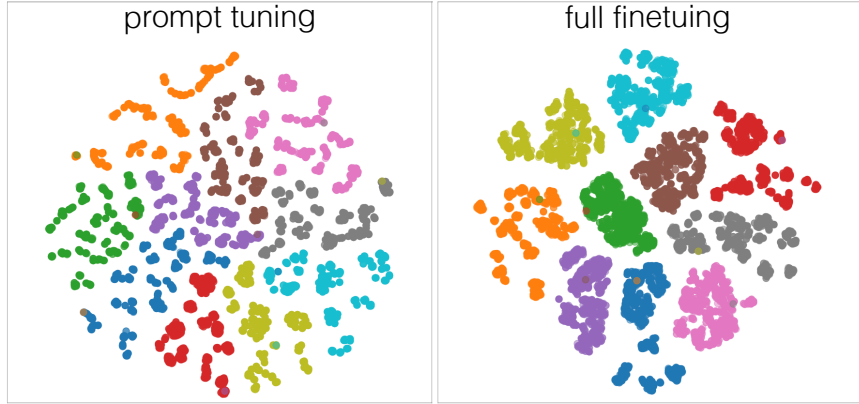


Figure 5: t-SNE visualizations of the embeddings before the decoder. The points of the same color denote the tasks with same language prompts, which are embedded together. The prompt tuning method could produce instruction-relevant features without updating vision backbone parameters.

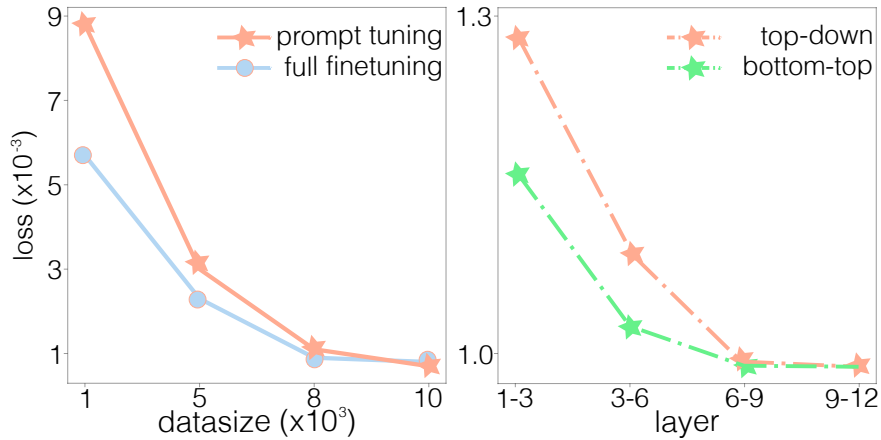


Figure 6: Ablation studies of prompt tuning. We investigate the effect of various design choices on affordance learning performance, including pretrained weights, decoder input, dataset size and prompt location.

4.1.3 Main Results

Table 1 presents the results of prompt tuning on our testing dataset for affordance learning, comparing against baselines. We use two metrics to evaluate our results: (i) L2 error of affordance heatmap estimation (the fourth column), and (ii) L2 distance between the predicted and ground truth of heatmap centers (the fifth column). For the second metric, we label the heatmap affordance of our data with 2D Gaussian blobs centered on the pixel of demonstrated action during data collection. For the inference, we fit Gaussian Mixture Models to determine the heatmap centers. The heatmap error is averaged on each map, and the center error is averaged on per center point.

Four observations could be made from this result: (i) The deep structure outperforms the other baselines except for the full finetuning. (ii) Full finetuning slightly outperforms deep prompt tuning in terms of heatmap estimation error and heatmap center error. However, the distinction of heatmap center errors (1.78 pixels) remains subtle, given the full image size of 224×224 . This outcome is favorable as it indicates that most heatmap errors are caused by the tails of the Gaussian distribution, instead of the center area where the robot actions actually applied on. (iii) As expected, the shallow structure performs suboptimally to the deep structure. In the following ablation studies, we will investigate how the prompt depth affects the performance. (iv) The training dataset only includes a manikin. We observe that it generates well on our testing data with real humans.

What do prompts learn? We show a t-SNE [Van der Maaten and Hinton, 2008] visualization of the embeddings after the last vision transformer layer and before the decoder in Fig. 5. We can see that the points of the same color (e. g., tasks with same language prompts) are embedded together, implying that the representations recover the underlying manifold structure of discriminative task information.

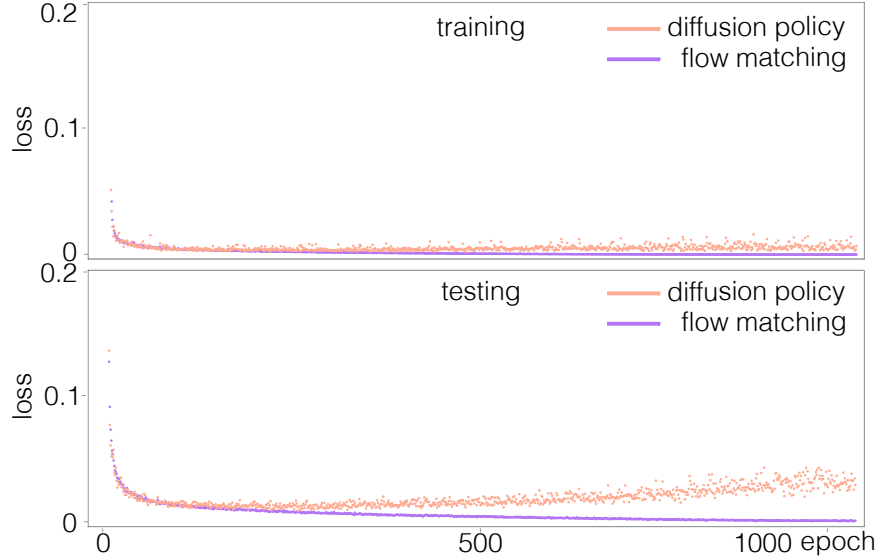


Figure 7: Training and testing loss of flow matching and diffusion policy throughout the training process. Flow matching exhibits greater stability on both training and evaluation than diffusion model.

4.1.4 Ablations

We further ablate model design choices.

Pretrained Weights. We evaluate using MAE self-supervised pretrained weights and supervised pretrained weights trained on ImageNet-21k dataset for the vision transformer model. The results in Table 1 show self-supervised pretrained weights perform better.

Decoder Input. We apply the decoder on the global output and image-corresponding output after the vision transformer respectively and report results in Table 1.

Dataset Size. We use various amounts of data to train the model. Fig. 6-left shows that prompt tuning has better adaptability than full finetuning when downstream data is scarce.

Prompt Location. We have seen different conclusions from prior works about whether the vision-language fusion should be integrated at early or late transformer layers. Thus we conduct experiments to insert prompts at various layers. From Fig. 6-right, we can see that inserting prompts to early layers (for example, layer 1-3 from bottom to top) achieves higher loss than inserting to late layers (for example, layer 1-3 from top to bottom). Thus in our case, prompts have greater significance at the late transformer layers. These results are also supported by the nature of vision transformer hierarchy: lower layers mainly capture low-level fundamental visual details, while higher layers focus on high-level concepts that might be vital for downstream tasks.

In conclusion, we observe no single method that outperforms all the rest. For scenarios where a small number of parameters or datasize is available, we reckon that prompt tuning remains the preferred approach.

4.2 Flow Matching Policy Evaluation

4.2.1 Baseline Studies

We compare our flow matching policy against two other robot behavior cloning methods: (i) *Diffusion Policy* [Chi et al., 2023], and (ii) *Transformer-based* behavior cloning with Mean Square Error Loss, as customary in RVT [Goyal et al., 2023], RT-X [Padalkar et al., 2023].

Note that we are aware of other well-performed robot behavior cloning methods, including energy-based IBC [Florence et al., 2022], GAIL [Ho and Ermon, 2016], etc. Since extensive studies have been conducted between these methods and diffusion policy, we choose two representative baselines for evaluation. We consider CNN-based and Transformer-based structures for flow matching. The input of flow matching and baselines are the RGB image with visual affordance, and the output is a complete long-horizon trajectory in both 2D pixel space and 3D Cartesian space. All 10 tasks in our

Methods		2D Trajectory Prediction (pixel) ↓	3D Trajectory Prediction (cm) ↓	Inference Times (ms) ↓
Baselines	Diffusion Policy (16-step)	0.890	2.096	110.72
	Transformer-based BC	2.797	6.109	7.59
Ours	Flow Matching (Transformer)	2.151	4.842	18.05
	Flow Matching (CNN, 1-step inference)	0.928	2.151	8.53
Ablations	Flow Matching (CNN, 4-step inference)	0.890	2.094	34.99
	Flow Matching (CNN, 8-step inference)	0.887	2.092	70.10
	Flow Matching (CNN, 16-step inference)	0.886	2.091	113.68
	Flow Matching (task-specific policy)	1.107	3.41	9.19

Table 2: Results of flow matching policy baseline and ablation studies. We report the error of 2D and 3D trajectory estimation and the average inference time. Our method achieves the best trajectory estimation accuracy, compared to other baselines. We also investigate the effect of various design choices on flow matching performance, including network structure and inference steps.

dataset are trained in a single policy with flow matching. For diffusion policy, we adopt the same setup as in the original paper [Chi et al., 2023], including 16 inference denoising iterations for real-world robot testing.

4.2.2 Main Results

Table 2 presents the results of flow matching policy on our testing dataset for robot trajectory learning, comparing against baselines. We use two metrics for evaluation: (i) the error of 2D and 3D trajectory estimation, and (ii) the average inference time across various steps, performed using PyTorch with RTX 4090 GPU acceleration. The trajectory error is averaged on each point of the trajectory. We use 32 waypoints to represent the trajectory. In the later session, we will ablate this choice.

Three observations could be made from this result: (i) Flow matching (CNN-based, 16 steps) outperforms other baselines in terms of 2D and 3D trajectory prediction accuracy. The 3D estimation performs decently with our method using only RGB images as input. But we also observe the 3D estimation could be highly attuned to camera angles. (ii) The Transformer behavior cloning achieves marginal precision. This is expected as it is hindered by the nature of multi-modal action distribution, causing the averaging out across non-convex spaces. (iii) Flow matching with 16 steps achieves slightly faster inference without loss of quality compared to diffusion policy with 16 steps. We hypothesize that flow matching with optimal transport generates straighter flows, and thus causes faster inference.

Fig. 1 showcases more examples of the waypoint motion path and vector field plots of flow matching policy. We could see that flow matching transforms random waypoints to the target trajectory from timestep 0 to 1. The animations in the supplementary video better demonstrate the whole process.

4.2.3 Comparisons against diffusion policy

Fig. 7 shows the training and testing loss of flow matching and diffusion policy throughout the training process. We can see flow matching exhibits greater stability on both training and evaluation than diffusion model. For the Push-T benchmark evaluation, flow matching also requires fewer steps and better performance (120 steps, score 1.0) to push a T-shaped block to fully overlap with a fixed target using a circular end-effector, compared to diffusion policy (200 steps, score 0.91).

4.2.4 Ablations

We further ablate various policy design choices.

Network Structure: As shown in Table 2, CNN-based flow matching achieves better results than transformer-based architecture. We hypothesize that transformer might need additional hyperparameter tuning.

Inference Steps: Table 2 also showcases better performances of flow matching when applying more inference steps, with a trade-off of longer inference time.

Trajectory Horizon: We empirically test trajectory representation with 8, 16, 32 and 64 waypoints. More waypoints are not necessary, while fewer waypoints are unable to entirely encapsulate the complete long-horizon trajectories. We



Figure 8: Examples of how visual affordance guides the flow matching policy.

Methods	Flow Matching	Diffusion Policy	Transformer BC	Flow Matching (separate policy)
Success Rate	0.82	0.76	0.44	0.80

Table 3: Success rate of real-world robot experiments.

have found out 32-waypoint trajectories to be optimal. In general, the trajectory horizon does not wield a significant influence on flow matching performance.

4.3 Real-World Robot Experiments

Lastly, we deploy flow matching and other policies on real robot manipulation evaluation, as shown in Table 3. We carry out 50 replications of trials for each policy. The orientation is predefined. We use a KINOVA Gen3 arm, an Azure Kinect camera, and a 3D printed UMI gripper [Chi et al., 2024] for real-world robot experiments.

We observe that most failures occurred during the initial grasping. Even the trajectory prediction is accurate in general, a slight misalignment between the first trajectory waypoint and the object would cause grasping failures. This problem might be addressed in the future by a weighted flow matching policy, which highlights the initial waypoints by adding higher probability weights. Since we have not considered closed-loop actions, the robot might also collide with objects in the process of moving to the first waypoint. Some out-of-distribution factors also lead to failure, including background and camera view changes. Larger data sizes and more diversity should alleviate this problem.

We also investigate how the affordance would guide the flow matching policy. We trained flow matching for each task separately, taking the raw RGB images as input. It achieves a higher loss but a similar success rate compared to training all tasks in one policy with affordance guidance. Interestingly, a further comprehensive examination reinforces the argument that flow matching could handle multimodal action distribution. Fig. 8 shows an example. From the left figure, we can see that when training a separate policy of moving the towel toward the trash for sweeping, the predicted trajectory (yellow) could be detached from the ground truth (red), but still a reasonable solution that allows for a successful robot execution. With affordance guidance, the prediction is closely aligned with the truth (Fig. 8-right).

5 Conclusion

We have formulated a prompt tuning method for affordance learning and flow matching policy for robot manipulation. The core idea of prompt tuning is to maximally exploit the pretrained foundation model, and rapidly excavate the relevance of foundation and downstream affordance learning tasks. Our focus in this work is not to outperform state-of-the-art general robot manipulation research. Instead, we have systematically studied flow matching framework, which provides an alternative to diffusion policy. The results suggest forsaking the stochastic construction in favor of more directly learning the probability path, allowing for improved generation. We qualitatively and quantitatively experiment on the multi-task robot manipulation scenarios to prove the ease of training and evaluation for flow matching. We could further improve performance by incorporating the robot state as an extra input of flow matching, estimating closed-loop

short horizon motions, and considering depth or pointcloud information for 3D orientation modeling. We leave these for future work.

References

- Abhishek Padalkar, Acorn Pooley, Ajinkya Jain, Alex Bewley, Alex Herzog, Alex Irpan, Alexander Khazatsky, Anant Rai, Anikait Singh, Anthony Brohan, et al. Open x-embodiment: Robotic learning datasets and rt-x models. *arXiv preprint arXiv:2310.08864*, 2023.
- Yecheng Jason Ma, William Liang, Guanzhi Wang, De-An Huang, Osbert Bastani, Dinesh Jayaraman, Yuke Zhu, Linxi Fan, and Anima Anandkumar. Eureka: Human-level reward design via coding large language models. *arXiv preprint arXiv:2310.12931*, 2023.
- Jacky Liang, Wenlong Huang, Fei Xia, Peng Xu, Karol Hausman, Brian Ichter, Pete Florence, and Andy Zeng. Code as policies: Language model programs for embodied control. In *2023 IEEE International Conference on Robotics and Automation (ICRA)*, pages 9493–9500. IEEE, 2023.
- Yen-Jen Wang, Bike Zhang, Jianyu Chen, and Koushil Sreenath. Prompt a robot to walk with large language models. *arXiv preprint arXiv:2309.09969*, 2023.
- Wenlong Huang, Chen Wang, Ruohan Zhang, Yunzhu Li, Jiajun Wu, and Li Fei-Fei. Voxposer: Composable 3d value maps for robotic manipulation with language models. *arXiv preprint arXiv:2307.05973*, 2023.
- Tete Xiao, Ilija Radosavovic, Trevor Darrell, and Jitendra Malik. Masked visual pre-training for motor control. *arXiv preprint arXiv:2203.06173*, 2022.
- Nils Ingelhart, Jesper Munkeby, Jonne van Haastregt, Anastasia Varava, Michael C Welle, and Danica Kragic. A robotic skill learning system built upon diffusion policies and foundation models. *arXiv preprint arXiv:2403.16730*, 2024.
- Menglin Jia, Luming Tang, Bor-Chun Chen, Claire Cardie, Serge Belongie, Bharath Hariharan, and Ser-Nam Lim. Visual prompt tuning. In *European Conference on Computer Vision*, pages 709–727. Springer, 2022.
- Edward J Hu, Yelong Shen, Phillip Wallis, Zeyuan Allen-Zhu, Yuanzhi Li, Shean Wang, Lu Wang, and Weizhu Chen. Lora: Low-rank adaptation of large language models. *arXiv preprint arXiv:2106.09685*, 2021.
- Pengfei Liu, Weizhe Yuan, Jinlan Fu, Zhengbao Jiang, Hiroaki Hayashi, and Graham Neubig. Pre-train, prompt, and predict: A systematic survey of prompting methods in natural language processing. *ACM Computing Surveys*, 55(9): 1–35, 2023.
- Kihyuk Sohn, Huiwen Chang, José Lezama, Luisa Polania, Han Zhang, Yuan Hao, Irfan Essa, and Lu Jiang. Visual prompt tuning for generative transfer learning. In *Proceedings of the IEEE/CVF Conference on Computer Vision and Pattern Recognition*, pages 19840–19851, 2023.
- Jiawen Zhu, Simiao Lai, Xin Chen, Dong Wang, and Huchuan Lu. Visual prompt multi-modal tracking. In *Proceedings of the IEEE/CVF conference on computer vision and pattern recognition*, pages 9516–9526, 2023.
- Yun Zhong and Yiannis Demiris. Dancemvp: Self-supervised learning for multi-task primitive-based dance performance assessment via transformer text prompting. In *Proceedings of the AAAI Conference on Artificial Intelligence*, volume 38, pages 10270–10278, 2024.
- Martin Maier and Rasha Abdel Rahman. No matter how: Top-down effects of verbal and semantic category knowledge on early visual perception. *Cognitive, Affective, & Behavioral Neuroscience*, 19:859–876, 2019.
- Fan Zhang and Yiannis Demiris. Learning garment manipulation policies toward robot-assisted dressing. *Science robotics*, 7(65):eabm6010, 2022.
- Mohit Shridhar, Lucas Manuelli, and Dieter Fox. Perceiver-actor: A multi-task transformer for robotic manipulation. In *Conference on Robot Learning*, pages 785–799. PMLR, 2023.
- Cheng Chi, Siyuan Feng, Yilun Du, Zhenjia Xu, Eric Cousineau, Benjamin Burchfiel, and Shuran Song. Diffusion policy: Visuomotor policy learning via action diffusion. *arXiv preprint arXiv:2303.04137*, 2023.
- Fan Zhang and Yiannis Demiris. Visual-tactile learning of garment unfolding for robot-assisted dressing. *IEEE Robotics and Automation Letters*, 2023.
- Fangchen Liu, Kuan Fang, Pieter Abbeel, and Sergey Levine. Moka: Open-vocabulary robotic manipulation through mark-based visual prompting. *arXiv preprint arXiv:2403.03174*, 2024.
- Ankit Goyal, Jie Xu, Yijie Guo, Valts Blukis, Yu-Wei Chao, and Dieter Fox. Rvt: Robotic view transformer for 3d object manipulation. In *Conference on Robot Learning*, pages 694–710. PMLR, 2023.
- James J Gibson. *The ecological approach to visual perception: classic edition*. Psychology press, 2014.

- Jonathan Ho and Stefano Ermon. Generative adversarial imitation learning. *Advances in neural information processing systems*, 29, 2016.
- Pete Florence, Corey Lynch, Andy Zeng, Oscar A Ramirez, Ayzaan Wahid, Laura Downs, Adrian Wong, Johnny Lee, Igor Mordatch, and Jonathan Tompson. Implicit behavioral cloning. In *Conference on Robot Learning*, pages 158–168. PMLR, 2022.
- Yaron Lipman, Ricky TQ Chen, Heli Ben-Hamu, Maximilian Nickel, and Matt Le. Flow matching for generative modeling. *arXiv preprint arXiv:2210.02747*, 2022.
- Tanmay Gupta, Amita Kamath, Aniruddha Kembhavi, and Derek Hoiem. Towards general purpose vision systems: An end-to-end task-agnostic vision-language architecture. In *Proceedings of the IEEE/CVF Conference on Computer Vision and Pattern Recognition*, pages 16399–16409, 2022.
- Alec Radford, Jong Wook Kim, Chris Hallacy, Aditya Ramesh, Gabriel Goh, Sandhini Agarwal, Girish Sastry, Amanda Askell, Pamela Mishkin, Jack Clark, et al. Learning transferable visual models from natural language supervision. In *International conference on machine learning*, pages 8748–8763. PMLR, 2021.
- Peng Gao, Shijie Geng, Renrui Zhang, Teli Ma, Rongyao Fang, Yongfeng Zhang, Hongsheng Li, and Yu Qiao. Clip-adapter: Better vision-language models with feature adapters. *International Journal of Computer Vision*, 132(2): 581–595, 2024.
- Xiao Liu, Kaixuan Ji, Yicheng Fu, Weng Lam Tam, Zhengxiao Du, Zhilin Yang, and Jie Tang. P-tuning v2: Prompt tuning can be comparable to fine-tuning universally across scales and tasks. *arXiv preprint arXiv:2110.07602*, 2021.
- Michael S Albergo and Eric Vanden-Eijnden. Building normalizing flows with stochastic interpolants. *arXiv preprint arXiv:2209.15571*, 2022.
- Max Braun, Noémie Jaquier, Leonel Rozo, and Tamim Asfour. Riemannian flow matching policy for robot motion learning. *arXiv preprint arXiv:2403.10672*, 2024.
- Xixi Hu, Bo Liu, Xingchao Liu, and Qiang Liu. Adaflow: Imitation learning with variance-adaptive flow-based policies. *arXiv preprint arXiv:2402.04292*, 2024.
- Quentin Rouxel, Andrea Ferrari, Serena Ivaldi, and Jean-Baptiste Mouret. Flow matching imitation learning for multi-support manipulation. *arXiv preprint arXiv:2407.12381*, 2024.
- Gabriel Peyré, Marco Cuturi, et al. Computational optimal transport: With applications to data science. *Foundations and Trends® in Machine Learning*, 11(5-6):355–607, 2019.
- Ethan Perez, Florian Strub, Harm De Vries, Vincent Dumoulin, and Aaron Courville. Film: Visual reasoning with a general conditioning layer. In *Proceedings of the AAAI conference on artificial intelligence*, volume 32, 2018.
- Kaiming He, Xiangyu Zhang, Shaoqing Ren, and Jian Sun. Deep residual learning for image recognition. In *Proceedings of the IEEE conference on computer vision and pattern recognition*, pages 770–778, 2016.
- Kaiming He, Xinlei Chen, Saining Xie, Yanghao Li, Piotr Dollár, and Ross Girshick. Masked autoencoders are scalable vision learners. In *Proceedings of the IEEE/CVF conference on computer vision and pattern recognition*, pages 16000–16009, 2022.
- Roy Ganz, Yair Kittenplon, Aviad Aberdam, Elad Ben Avraham, Oren Nuriel, Shai Mazor, and Ron Litman. Question aware vision transformer for multimodal reasoning. In *Proceedings of the IEEE/CVF Conference on Computer Vision and Pattern Recognition*, pages 13861–13871, 2024.
- Yunfan Jiang, Agrim Gupta, Zichen Zhang, Guanzhi Wang, Yongqiang Dou, Yanjun Chen, Li Fei-Fei, Anima Anandkumar, Yuke Zhu, and Linxi Fan. Vima: General robot manipulation with multimodal prompts. *arXiv preprint arXiv:2210.03094*, 2(3):6, 2022.
- Laurens Van der Maaten and Geoffrey Hinton. Visualizing data using t-sne. *Journal of machine learning research*, 9 (11), 2008.
- Cheng Chi, Zhenjia Xu, Chuer Pan, Eric Cousineau, Benjamin Burchfiel, Siyuan Feng, Russ Tedrake, and Shuran Song. Universal manipulation interface: In-the-wild robot teaching without in-the-wild robots. In *Proceedings of Robotics: Science and Systems (RSS)*, 2024.